

# Effect of Tumor-Pixel Positioning on the Variability of SUV Measurements in PET Images

Koji Itagaki\*, Katsuhiko Mitsumoto, Masaaki Kajisako, Maki Shioji, Shigeto Kawase

Division of Clinical Radiology Service, Kyoto University Hospital, Kyoto, Japan

## ARTICLE INFO

Article type:  
Original article

### Article history:

Received: 18 Nov 2021  
Revised: 4 Feb 2022  
Accepted: 19 Feb 2022

### Keywords:

PET/MR  
SUV measurement  
Reproducibility

## ABSTRACT

**Objective(s):** The aim of this study was to investigate the effect on standardized uptake value (SUV) measurement variability of the positional relationship between objects of different sizes and the pixel of a positron emission tomography (PET) image.

**Methods:** We used a NEMA IEC body phantom comprising six spheres with diameters of 10, 13, 17, 22, 28, and 37 mm. The phantom was filled with  $^{18}\text{F}$  solution and contained target-to-background ratios (TBRs) of 2, 4, and 8. The PET data were acquired for 30 min using a SIGNA PET/MR scanner. The PET images were reconstructed with the ordered subsets expectation maximization (OSEM) algorithm with and without point-spread function (PSF) correction (OSEM + PSF + Filter and OSEM + Filter, respectively). A Gaussian filter of 4 mm full width at half maximum was applied in all reconstructions, except for one model (OSEM + PSF + no Filter). The matrix sizes were  $128 \times 128$ ,  $192 \times 192$ ,  $256 \times 256$  and  $384 \times 384$ . Reconstruction was performed by shifting the reconstruction center position by 1 mm in the range 0 to 3 mm in the upward or rightward direction for each parameter. For all reconstructed images, the  $\text{SUV}_{\text{max}}$  of each hot sphere was measured. To investigate the resulting variation in the  $\text{SUV}_{\text{max}}$ , the coefficient of variation (CV) of each  $\text{SUV}_{\text{max}}$  was calculated.

**Results:** The CV of the  $\text{SUV}_{\text{max}}$  increased as the matrix size and the diameter of the hot sphere decreased in all reconstruction settings. With PSF correction, the CV of  $\text{SUV}_{\text{max}}$  increased as the TBR increased except when the TBR was 2. The CV of the  $\text{SUV}_{\text{max}}$  measured in the OSEM + PSF + no Filter images were larger than those measured in the OSEM + PSF + Filter images. The amount of this increase was higher for smaller spheres and larger matrix sizes and was independent of TBR.

**Conclusions:** Shifting the reconstruction center position of the PET image causes variability in  $\text{SUV}_{\text{max}}$  measurements. To reduce the variability of SUV measurements, it is necessary to use sufficient matrix sizes to satisfy sampling criterion and appropriate filters.

► Please cite this paper as:

Itagaki K, Mitsumoto K, Kajisako M, Shioji M, Kawase Sh. Effect of Tumor-Pixel Positioning on the Variability of SUV Measurements in PET Images. Asia Ocean J Nucl Med Biol. 2023; 11(1): 71-81. doi: 10.22038/AOJNMB.2022.61623.1434

## Introduction

Malignant tumors are often detected and staged using  $^{18}\text{F}$ -fluoro-2-deoxy-D-glucose ( $^{18}\text{F}$ -FDG) positron emission tomography (PET) (1). In FDG-PET, visual assessment is widely used to diagnose malignancy, but semi-quantitative analysis using a standardized uptake value (SUV) is also used (2, 3). SUVs are also an important tool for monitoring the response to therapy of various malignant tumors (4).

However, many biological and technological factors affect SUV measurements (5).  $\text{SUV}_{\text{max}}$  has higher interobserver reproducibility, which is important for multicenter studies evaluating the usefulness of  $^{18}\text{F}$ -FDG PET for treatment monitoring (6), but because  $\text{SUV}_{\text{max}}$  is sensitive to noise, the within-patient SD for  $\text{SUV}_{\text{max}}$  is higher in noisy conditions than that for  $\text{SUV}_{\text{mean}}$  or  $\text{SUV}_{\text{peak}}$  (5,7,8,9). However,  $\text{SUV}_{\text{max}}$  is still widely used because it can be easily measured

\* Corresponding author: Koji Itagaki. Kyoto University Hospital, Division of Clinical Radiology Service, 54 Shogoin-kawahara-cho, Sakyo-ku, Kyoto 606-8507, Japan. Tel: 075-751-3522; Email: itagaki415@gmail.com

© 2023 mums.ac.ir All rights reserved.

This is an Open Access article distributed under the terms of the Creative Commons Attribution License (<http://creativecommons.org/licenses/by/3.0>), which permits unrestricted use, distribution, and reproduction in any medium, provided the original work is properly cited.

from any workstation and avoid inclusion of necrotic or other non-tumor elements (10-12).

The mean absolute percentage difference between successive SUV<sub>max</sub> measurements has been reported to be 13%±12 (10) and 11.3%±8.0 (13). Another group reported that the within-patient SD for SUV<sub>max</sub> varied from 10.7% to 12.8% (14). In addition, the within-patient SD for SUV<sub>max</sub> including only the effects of image noise was reported to be 5.6%±0.9 (7).

Recent advancements in the hardware and software of PET devices, such as reductions in detector size, increases in signal-to-noise ratio using time-of-flight (TOF) techniques, and improvements in spatial resolution using point-spread function (PSF) reconstruction have improved the detectability of small lesions (15).

In addition, it has been reported that the detectability of small lesions is improved with long acquisition durations (8), which should also enable small lesions to be clearly delineated in PET/MR generally. SUV measurement in small lesions is, however, often affected by the partial volume effect (PVE) (9).

PVE in PET image mainly results from the finite spatial resolution of the imaging system and image sampling, and occurs whenever the tumor size is less than three times the full width half maximum (FWHM) of the spatial resolution (8). The spatial resolution in PET images is limited by the physical size of detector, positron range, radius of the tomograph detector ring, and reconstruction method (16). As for the reconstruction methods, increasing the number of iterations improves the spatial resolution because higher frequencies can be recovered (17), which may improve the detection of small lesions, but also increase image noise (18). In PET/MR, a longer acquisition duration reduces image noise and enables the use of reconstruction methods with higher spatial resolutions. By contrast, in image sampling, large pixels are more likely to underestimate the SUV. Moreover, it has been reported that there is variability in SUV<sub>max</sub> depending on the positional relationship between the object and the pixel of the PET image (5). Maebatake et al. reported that the repeatability of a small hot spot was affected by the positional relationship between the subject and pixels (19). However, the variability of SUV measurements due to the positional relationship may also depend on the size of the object as well as the finite spatial resolution of the imaging system.

The aim of the present study was to investigate the effect of the positional relationship between objects of different sizes and the pixels of the PET image on the variability of SUV measurements using a

National Electrical Manufacturers Association (NEMA) International Electrotechnical Commission (IEC) body phantom.

## Methods

### Phantom

We used a NEMA IEC body phantom comprising six spheres with diameters of 10, 13, 17, 22, 28, and 37 mm. All spheres and the background of the phantom were filled with <sup>18</sup>F solution. The phantom contained target-to-background ratios (TBRs) of 2, 4, and 8 on a background of 5.3 kBq/mL of radioactivity concentration, according to the Japanese guidelines for oncological <sup>18</sup>F-FDG PET/CT data acquisition (20).

### Data Acquisition

PET data were acquired using a PET/MR scanner (SIGNA PET/MR; GE Healthcare) with silicon photomultipliers (SiPMs) and TOF-PET capability. This PET scanner comprised five rings with a total of 20,160 lutetium-based scintillation crystals with dimensions of 4.0×5.3×25 mm<sup>3</sup>. Sinogram plane had 224 (radial coordinate) ×357 (azimuthal angle) bins, as no transverse mashing was applied. This system had axial and transaxial fields of view of 25 and 60 cm, respectively. The coincidence time window was 4.57 ns. The TOF timing resolution is 386 ps. The spatial resolutions at 1 and 10 cm from the center of the field of view were 4.2 and 5.2 mm in FWHM, respectively. The PET data were acquired in 3-dimensional list mode for 30 min.

### Image reconstruction

PET images were reconstructed using a 3-dimensional ordered subsets expectation maximization (OSEM) algorithm with PSF correction (OSEM + PSF + Filter) using four iterations and 16 subsets. A Gaussian filter of 4 mm FWHM was applied in the reconstruction. The reconstruction parameters were determined according to the clinical setting for PET/MR examinations with an acquisition time of fifteen to twenty minutes. To investigate the effect of matrix size on the variability of SUV measurements due to the positional relationship, we reconstructed PET images with matrix size of 128×128, 192×192, 256×256, and 384×384. Pixel sizes were 4.7×4.7, 3.1×3.1, 2.3×2.3, and 1.6×1.6 mm, respectively. Although large pixel sizes may violate the sampling criterion, the commercial reconstruction software allows the selection of matrix size of 128×128 or 192×192, which may be used. In addition, to evaluate the effect of PSF correction on its variability, we reconstructed PET images

without PSF correction (OSEM + Filter). No post-smoothing was applied in one OSEM+PSF model (OSEM + PSF + no Filter) to evaluate the effect of the post-smoothing filter. All PET images were reconstructed with TOF information. The PET image slice thickness was 2.78 mm. The scatter correction was conducted using single scatter simulation, and the attenuation correction was performed using CT

measurement-based attenuation templates. To vary the relationship between the subject and the pixel of the PET image, reconstruction was performed while shifting the reconstruction center position in intervals of 1 mm from 0 to 3 mm in the upward or rightward direction for each parameter (Figure 1). Therefore, for each reconstruction parameter, 16 sets of images were reconstructed.

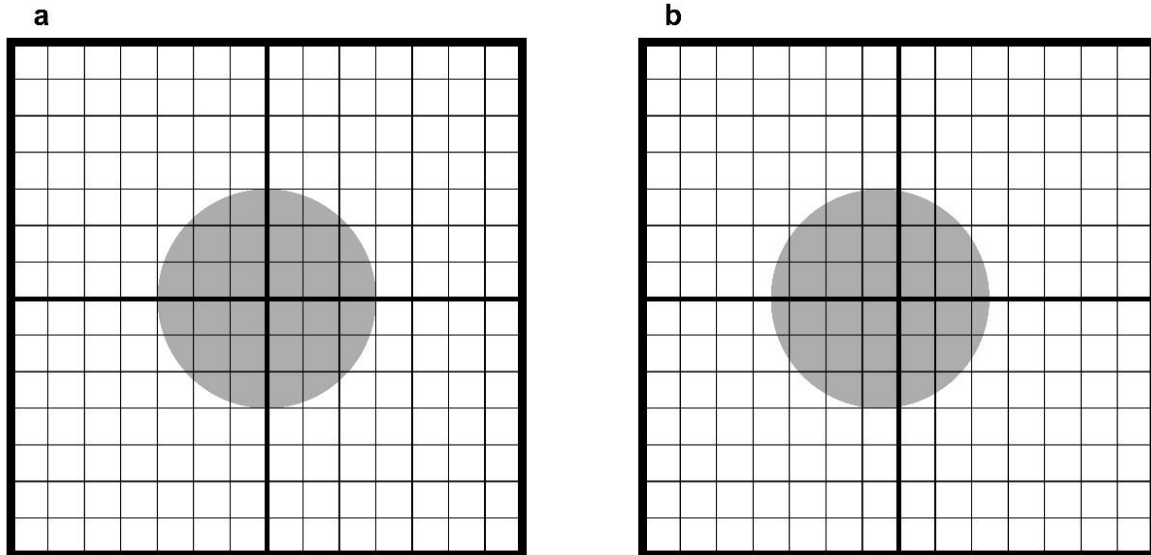


**Figure 1.** Reconstructed image without (a) and with (b) a rightward shift in the reconstruction center position. The grid represents the image matrix, and the gray sphere represents the hot sphere

### Data analysis

All PET datasets were analyzed using an Advantage Workstation (GE Healthcare). For all reconstructed images, the  $SUV_{max}$  of each hot sphere was determined from a spherical volume of interest with a diameter large enough to include each hot sphere.

To investigate the variation in the  $SUV_{max}$  of each hot sphere when the reconstruction center position was shifted, the coefficient of variation (CV) of  $SUV_{max}$  was calculated using the following equation.

$$CV = \frac{\sigma}{SUV_{max}} \times 100 (\%)$$

Here,  $\sigma$  and  $\overline{SUV_{max}}$  are respectively the standard deviation and mean of the  $SUV_{max}$  of each measured hot sphere.

### Results

The  $SUV_{max}$  of each hot sphere measured in the OSEM + PSF + Filter images with different matrix sizes and shifted reconstruction center positions at each TBR are shown in Figure 2. The difference between the maximum and minimum  $SUV_{max}$  ( $\Delta SUV_{max}$ ) of the 10-mm hot sphere increased as the matrix size decreased. The CV of the  $SUV_{max}$  of each hot sphere measured in the OSEM + PSF + Filter images with different matrix sizes at each TBR are shown in Table 1. The CV of increased as matrix size decreased, sphere diameter decreased, and TBR increased. The CV of the 10-mm hot sphere were 13.82%, 5.14%, 2.91%, and 1.18% at a TBR of 8 for matrix sizes of 128, 192, 256, and 384, respectively.

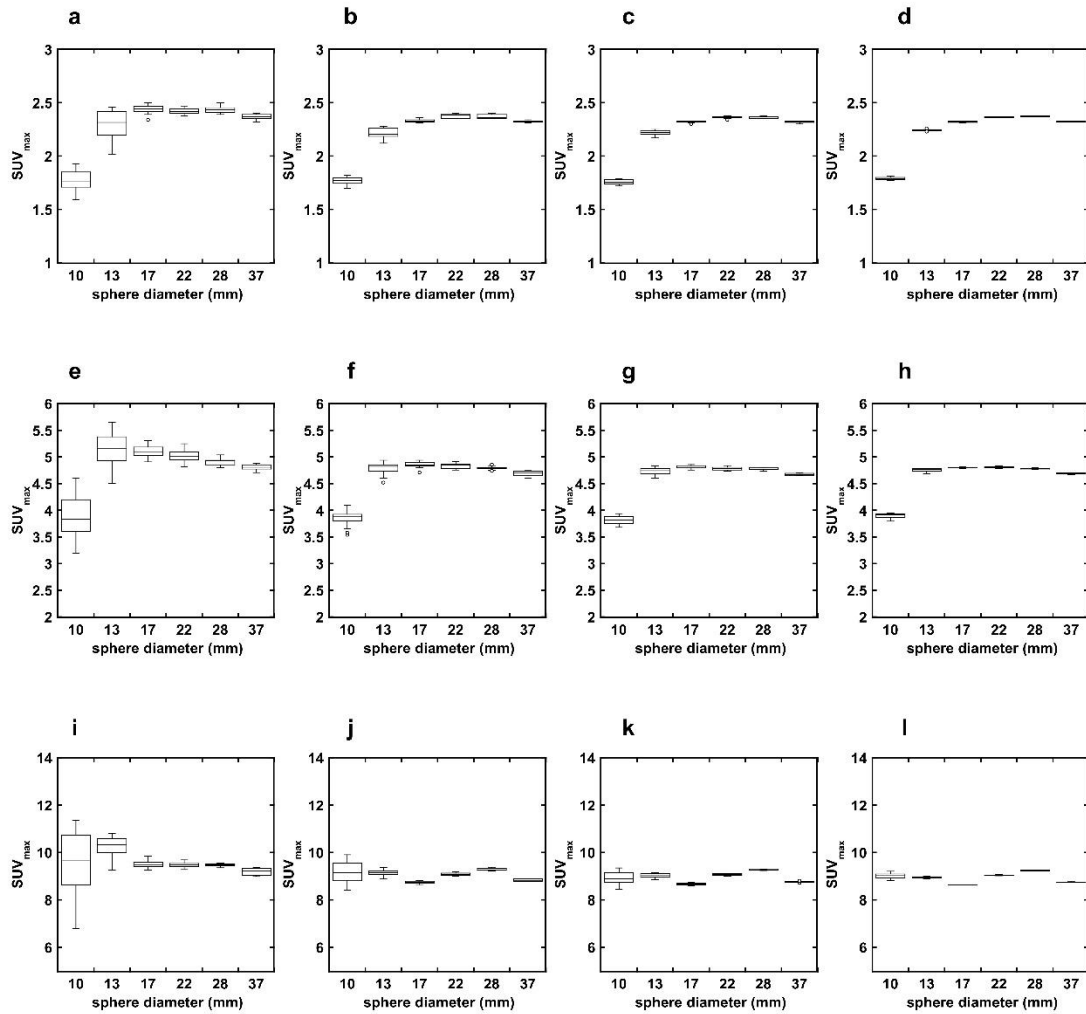


**Figure 2.** Relationship between sphere size and  $SUV_{max}$  at different matrix sizes in the OSEM + PSF + Filter images. The matrix sizes are 128 (a, e, i), 192 (b, f, j), 256 (c, g, k), and 384 (d, h, l) at a TBR of 2 (upper row), 4 (middle row), and 8 (lower row). The  $\Delta SUV_{max}$  was higher for smaller matrix sizes and smaller diameters of the hot sphere

**Table 1.** CV of  $SUV_{max}$  in the OSEM + PSF + Filter images for different matrix sizes at each TBR

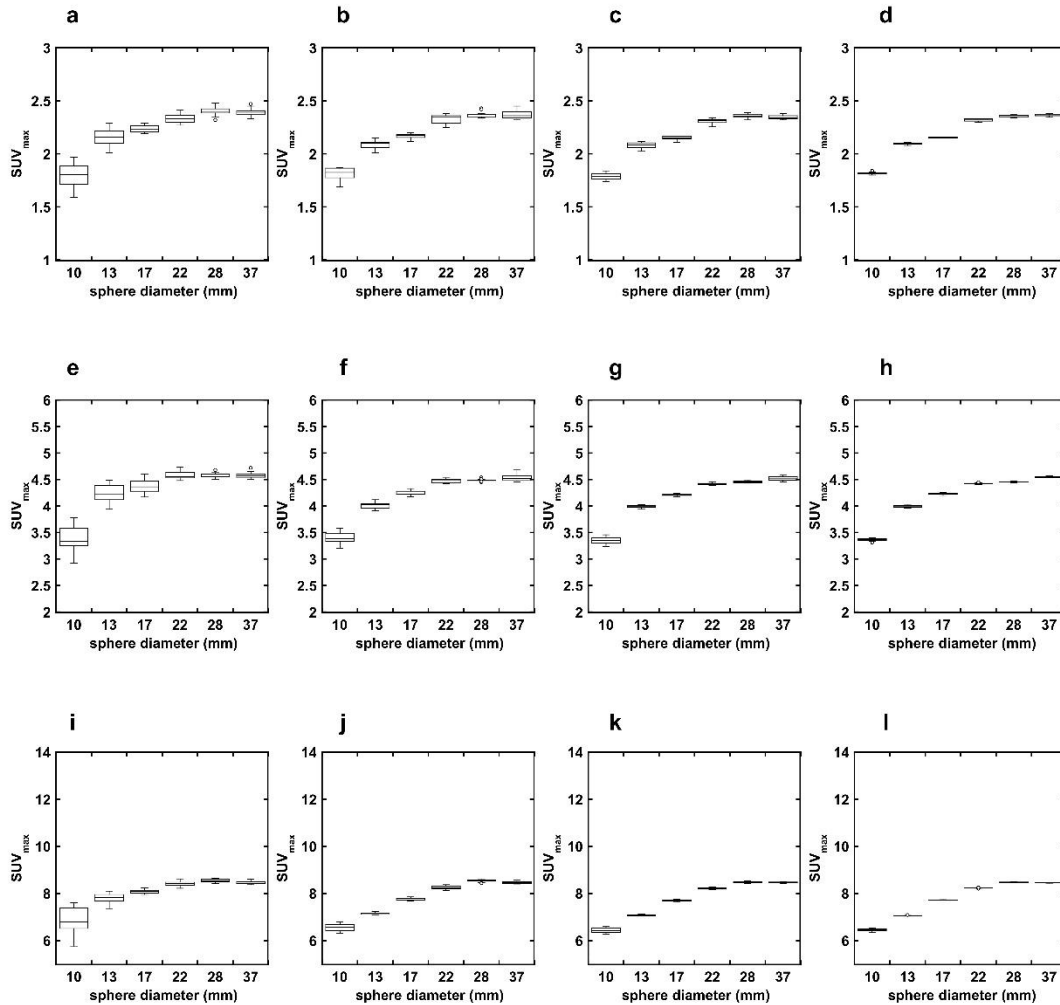
TBR	Spere diameter (mm)	Matrix size			
		128	192	256	384
2	10	5.55	1.85	1.27	0.57
	13	5.41	2.15	1.01	0.35
	17	1.56	0.63	0.36	0.34
	22	0.96	0.77	0.41	0.20
	28	1.19	0.78	0.47	0.21
	37	0.95	0.42	0.40	0.21
4	10	10.13	4.13	2.15	1.02
	13	5.91	2.49	1.31	0.67
	17	2.31	1.16	0.59	0.25
	22	2.18	1.07	0.63	0.33
	28	1.29	0.64	0.48	0.19
	37	1.00	0.97	0.38	0.25
8	10	13.82	5.14	2.91	1.18
	13	4.26	1.41	0.94	0.29
	17	1.57	0.56	0.52	0.13
	22	1.07	0.64	0.43	0.16
	28	0.50	0.55	0.15	0.13
	37	1.57	0.59	0.24	0.13

Figure 3 shows the  $SUV_{max}$  of each hot sphere measured in the OSEM + Filter images with different matrix sizes and shifted reconstruction center positions at each TBR.

The  $SUV_{max}$  of the 10-mm hot sphere measured in OSEM + Filter images was smaller than that measured in the OSEM + PSF + Filter images at TBRs of 4 and 8. The CV of the  $SUV_{max}$  of each hot

sphere measured in the OSEM + Filter images with different matrix sizes at each TBR are shown in Table 2. The CV of  $SUV_{max}$  increased as matrix size and sphere decreased, but was

independent of TBR. The CV of the 10-mm hot sphere were 7.83%, 2.20%, 1.67%, and 0.66% at a TBR of 8 for matrix sizes of 128, 192, 256, and 384, respectively.



**Figure 3.** Relationship between sphere size and  $SUV_{max}$  at different matrix sizes in the OSEM + Filter images (without PSF). The matrix sizes are 128 (a, e, i), 192 (b, f, j), 256 (c, g, k), and 384 (d, h, l) at a TBR of 2 (upper row), 4 (middle row), and 8 (lower row). The  $\Delta SUV_{max}$  was lower than in the OSEM + PSF + Filter images (Figure 2) with smaller diameters of the hot sphere at a TBR of 4 and 8

**Table 2.** CV of  $SUV_{max}$  in the OSEM + Filter images (without PSF) for different matrix sizes at each TBR

TBR	Sphere diameter (mm)	Matrix size			
		128	192	256	384
2	10	5.67	2.92	1.76	0.57
	13	3.73	1.69	1.24	0.48
	17	1.42	1.00	0.82	0.23
	22	1.77	1.82	0.94	0.39
	28	1.62	1.02	0.78	0.41
	37	1.46	1.62	0.80	0.39
4	10	7.57	3.18	1.92	0.81
	13	3.82	1.47	0.59	0.42
	17	2.95	0.95	0.39	0.32
	22	1.67	0.87	0.38	0.24
	28	1.04	0.46	0.36	0.18
	37	1.24	1.34	0.83	0.26
8	10	7.83	2.20	1.67	0.66
	13	2.53	0.50	0.31	0.21
	17	0.98	0.59	0.31	0.15
	22	1.21	0.88	0.45	0.14
	28	0.76	0.61	0.40	0.18
	37	0.71	0.60	0.26	0.12

Figure 4 shows the  $SUV_{max}$  of each hot sphere measured in the OSEM + PSF + no Filter images with different matrix sizes and shifted reconstruction center positions at each TBR. The CV of  $SUV_{max}$  of each hot sphere measured in the OSEM + PSF + no Filter images with different matrix sizes at each TBR are shown in Table 3. These results are larger than those of

the OSEM + PSF + Filter images. The degree of increase in CV was higher for smaller spheres and larger matrix sizes, but was independent of TBR. The CV of the 10-mm hot sphere were 14.39%, 6.89%, 4.52%, and 1.83% at a TBR of 8 for matrix sizes of 128, 192, 256, and 384, respectively.

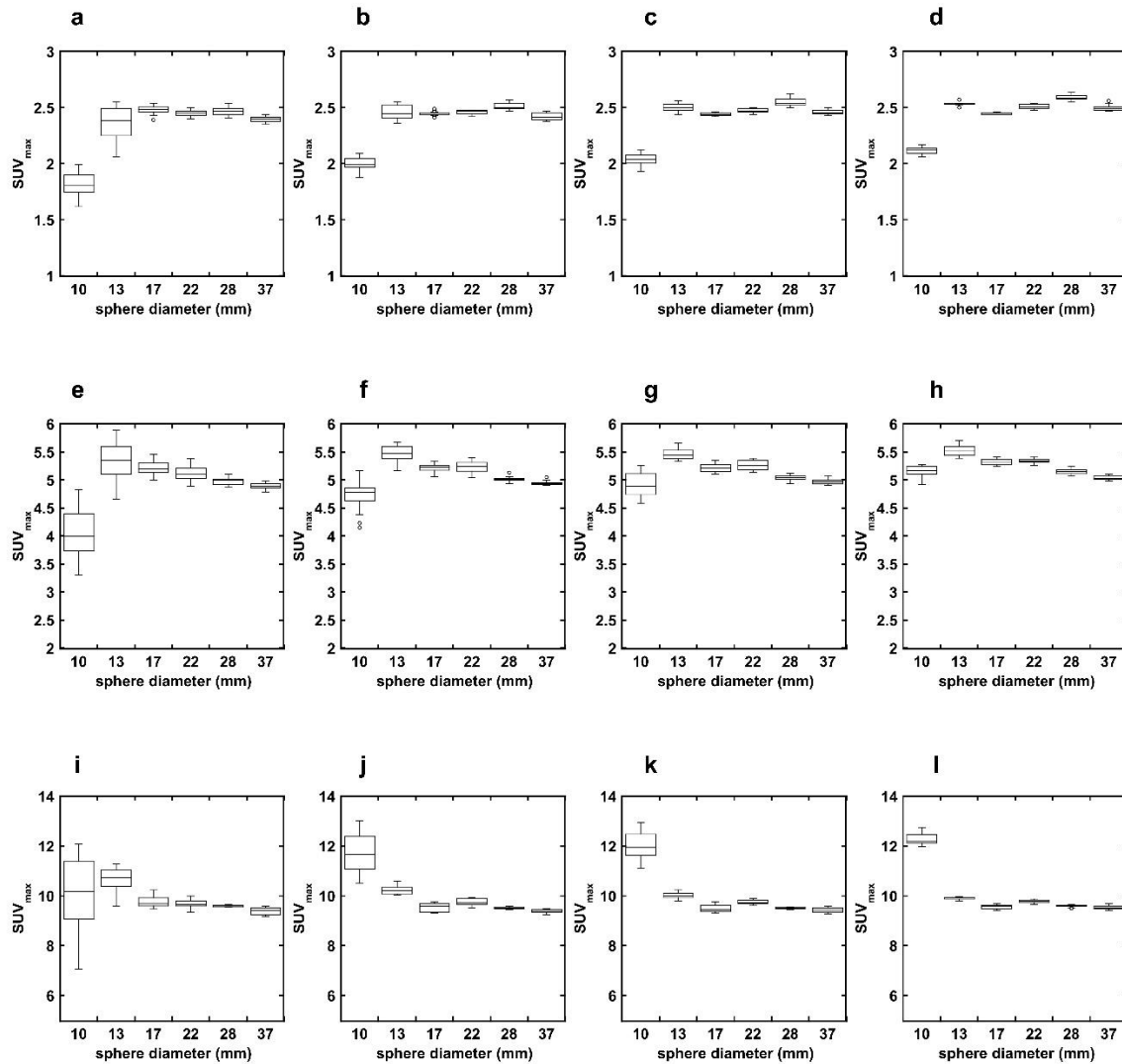


**Figure 4.** Relationship between sphere size and  $SUV_{max}$  at different matrix sizes in the OSEM + PSF + no Filter images. The matrix sizes are 128 (a, e, i), 192 (b, f, j), 256 (c, g, k), and 384 (d, h, l) at a TBR of 2 (upper row), 4 (middle row), and 8 (lower row). The  $\Delta SUV_{max}$  was higher than in the OSEM + PSF + Filter images (Figure 2)

**Table 3.** CV of SUV<sub>max</sub> in the OSEM + PSF + no Filter images for different matrix sizes at each TBR

TBR	Sphere diameter (mm)	Matrix size			
		128	192	256	384
2	10	5.93	2.76	2.49	1.45
	13	5.77	2.50	1.27	0.72
	17	1.52	0.82	0.50	0.23
	22	1.01	0.81	0.77	0.79
	28	1.43	1.19	1.44	0.99
	37	1.04	1.29	0.86	1.02
4	10	10.70	6.05	4.21	1.81
	13	6.14	2.93	1.77	1.64
	17	2.49	1.24	1.42	0.92
	22	2.46	1.96	1.67	0.82
	28	1.29	0.89	0.93	0.97
	37	1.11	0.87	0.91	0.76
8	10	14.39	6.89	4.52	1.83
	13	4.45	1.54	1.12	0.40
	17	2.13	1.75	1.57	0.84
	22	1.62	1.32	0.84	0.67
	28	0.34	0.36	0.33	0.46
	37	1.50	0.71	1.03	0.67

## Discussion

In this study, we investigated the effect of the positional relationship between an object and a pixel of a PET image on the variability of SUV measurements. To change the relationship between the subject and the pixels of PET images, we reconstructed PET images by shifting the reconstruction center position by 1 mm in the upward or rightward direction.

Shifting this reconstruction center position causes variability in SUV<sub>max</sub> measurements. The degree of variation depends on the reconstruction conditions (matrix size, post-smoothing filter, and PSF correction) as well as TBR. Biological factors, scanner variability, and reconstruction parameters will affect SUV measurements (5). In this study, the same emission data were used for each TBR to minimize the effects of phantom preparation and placement accuracy. We also acquired the data over a long duration to reduce the effect of statistical noise. Therefore, the main cause of the variability in SUV<sub>max</sub> in this study appears to be PVE related to image sampling. The CV of SUV<sub>max</sub> increased as matrix size and the diameter of the hot sphere decreased because of the increase in PVE related to image sampling.

The measurement of small lesions is particularly affected by PVE, and PET counts are underestimated when the image of the hot sphere lies between certain pixels (Figure 5) (8). Another reason for the increase of the CV of

SUV<sub>max</sub> might be due to the change in the influence of spill-out and aliasing depending on of the positional relationship between hot spheres and a pixel. With larger pixel sizes, their effect might be significant (8).

With PSF correction, the CV of SUV<sub>max</sub> increased with increases in TBR as well as with decreases in matrix size and the diameter of the hot sphere. One cause of the increase in variability of SUV<sub>max</sub> with PSF correction seems to be edge artifacts due to PSF correction. For small spheres, this artifact was observed as a sharp peak at the center of spheres that increased the PVE related to image sampling (16,17). At lower TBRs, the edge artifact was less likely to appear, so the CV of SUV<sub>max</sub> did not increase as much (17).

In addition, for the same TBR, the CV of SUV<sub>max</sub> decreased when no PSF correction was used, except when the TBR was 2. It has been reported that the variability in SUV measurement increases with PSF correction (16). Munk et al. reported that the lumpy noise caused by PSF correction decreases the reproducibility of SUV measurement (21).

Moreover, PET images without PSF correction are more blurred than those with PSF correction, resulting in reduced PVE and decreased variability. At a TBR of 2, two factors can be considered the reasons the CV of SUV<sub>max</sub> does not decrease when no PSF correction is used.

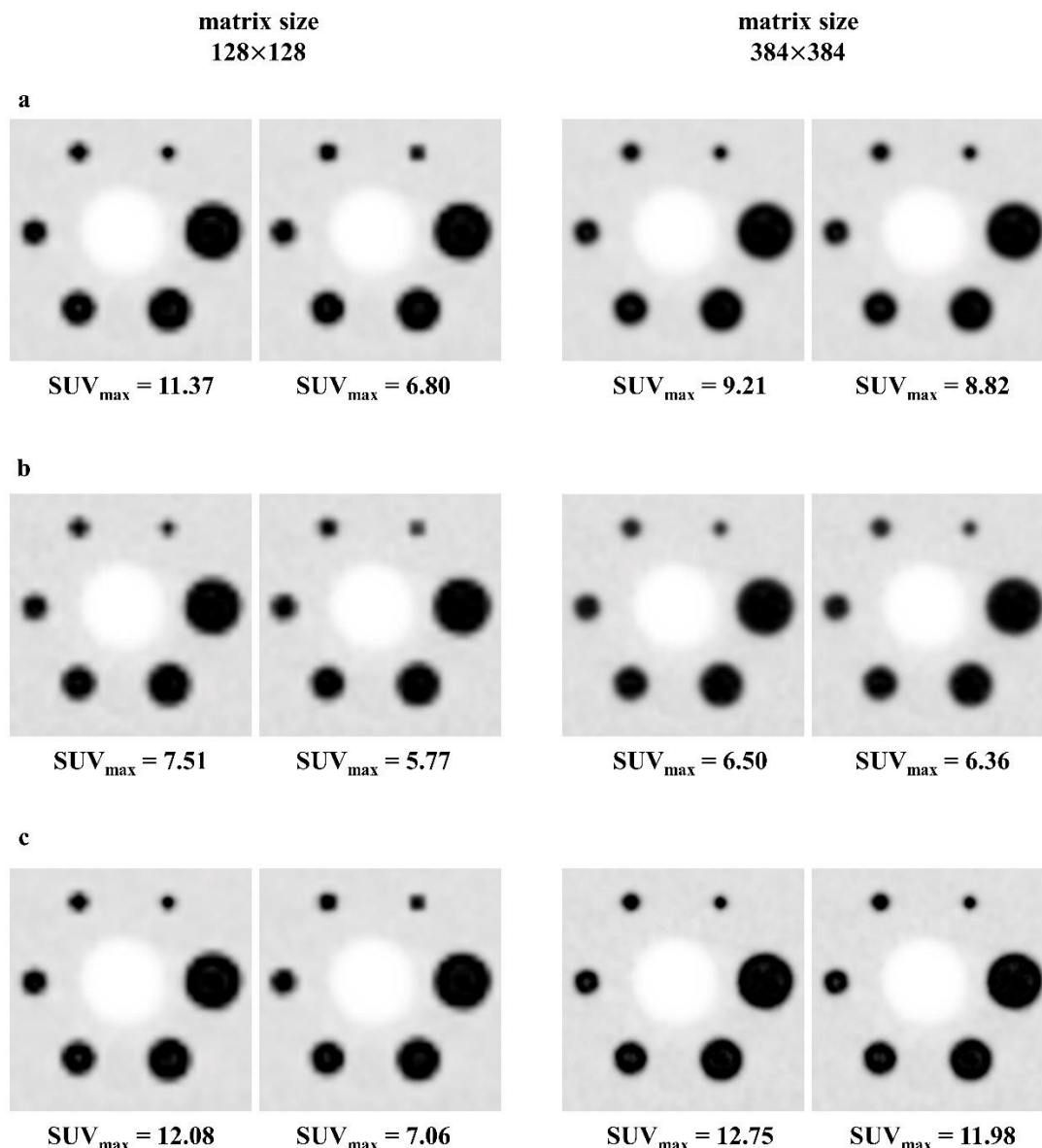


**Figure 5.** PET images reconstructed at different reconstruction center position. Matrix sizes are 128×128 and 384×384 at a TBR of 8. The images reconstructed with OSEM + PSF + Filter (a), OSEM + Filter (without PSF) (b), OSEM + PSF + no Filter (c). The values at the bottom of the images are the maximum and minimum  $SUV_{max}$  of the 10-mm hot sphere for each reconstruction settings

The first factor is the improvement in spatial resolution obtained by PSF correction, which is dependent on concentration. At a low TBR, the resolution is not as improved as it is at high TBR, so PET images taken at low TBRs are blurrier (17, 22, 23). Therefore, the results were less affected by PVE related to image sampling. The second factor is the improvement in signal-to-noise ratio caused by PSF correction (24). In the hot sphere at a low TBR, image noise is relatively high due to the low concentration of radioactivity, and the CV of  $SUV_{max}$  increased, especially when PSF correction was not used. Without PSF correction, the higher CV of  $SUV_{max}$  of the 37 mm sphere, which should have been less sensitive to PVE, indicates that image noise

is one factor affecting the variation at a TBR of 2. Note that the use of PSF correction has been reported to improve the detectability of small lesions (25, 26). The trade-off between lesion detectability and the accuracy of SUV measurement must be considered when determining the reconstruction parameters.

The CV of the  $SUV_{max}$  measured in the OSEM + PSF + no Filter images was larger than that measured in the OSEM + PSF + Filter images.

The degree of increase in CV of  $SUV_{max}$  was higher for smaller spheres and larger matrix sizes but independent of TBR. Without post-smoothing, the measurement of the PET counts was more affected by PVE related to image sampling because of the sharper profile of the

hot sphere, resulting in a larger variation in small spheres when the reconstruction center position was shifted.

For large matrix sizes,  $SUV_{max}$  is higher because of increased image noise. This can be suppressed by applying a post-smoothing filter (27, 28). Recently, several studies reported that the detectability of small lesions improves with the use of larger matrix sizes (15, 25, 29). Another study reported that reconstruction parameters affect the SUV measurement of small lesions (26). When evaluating small lesion uptake, it is necessary to increase the matrix size sufficiently to reduce the variability caused by PVE related to image sampling and to use an optimal post-smoothing filter to prevent overestimation of  $SUV_{max}$  due to image noise. In this study, we applied the fixed filter size at 4 mm FWHM to evaluate the effect of the post-smoothing filter. However, in clinical practice, it is necessary to use the optimal filter for the pixel size.

Several groups have evaluated the reproducibility of SUV measurements (7, 10, 13, 14). They reported that the CV of  $SUV_{max}$  was approximately 8.0%–13%. Those studies did not mention the tumor size, but in the present study, the CV of  $SUV_{max}$  reached 14.39% using the same phantom data and reconstruction parameters. Therefore, the variability in  $SUV_{max}$  caused by shifting the reconstruction center position is considered to be an important factor in SUV measurement.

The present study has several limitations. First, the target objects we measured were spherical and homogeneous. PVE depends on the shape and homogeneity of the tumor (8). A simulation study may address this limitation. Second, the PSF correction is position dependent, and the degree of variation may change depending on the position of the hot sphere. In addition, a long acquisition time of 30 minutes was used to exclude the effect of statistical noise on the variability of SUV measurements in this study, but further evaluation with actual clinical acquisition time is necessary. Finally, we evaluated the variability of  $SUV_{max}$  due to the positional relationship, but  $SUV_{mean}$  and  $SUV_{peak}$  are also an important tool for monitoring the response to therapy of malignant tumors and needs to be evaluated in the future (30, 31).

## Conclusion

Shifting the reconstruction center position in PET image reconstruction causes variability in  $SUV_{max}$  measurements. To reduce the variability of SUV measurements, it is necessary to use

sufficient matrix sizes to satisfy sampling criterion and appropriate filters.

## Acknowledgments

We thank Kimberly Moravec, PhD, from Edanz (<https://jp.edanz.com/ac>) for editing a draft of this manuscript.

## Conflict of interest

The authors declare that they have no conflicts of interest.

## References

1. Fletcher JW, Djulbegovic B, Soares HP, Siegel BA, Lowe VJ, Lyman GH, et al. Recommendations on the use of  $^{18}F$ -FDG PET in oncology. *J Nucl Med.* 2008; 49(3):480-508.
2. Johnson SA, Kumar A, Matasar MJ, Schöder H, Rademaker J. Imaging for staging and response assessment in lymphoma. *Radiology.* 2015; 276(2):323-38.
3. Lin C, Itti E, Haioun C, Petegnief Y, Luciani A, Dupuis J, et al. Early  $^{18}F$ -FDG PET for prediction of prognosis in patients with diffuse large B-cell lymphoma: SUV-based assessment versus visual analysis. *J Nucl Med.* 2007; 48(10):1626-32.
4. Weber BWA, Petersen V, Schmidt B, Tyndale-hines L, Link T, Peschel C. Positron Emission Tomography in Non – Small-Cell Lung Cancer: Prediction of Response to Chemotherapy by Quantitative Assessment of Glucose Use. *J Clin Oncol.* 2003; 21(14): 2651-7.
5. Adams MC, Turkington TG, Wilson JM, Wong TZ. A systematic review of the factors affecting accuracy of SUV measurements. *Am J Roentgenol.* 2010; 195(2):310-20 .
6. Benz MR, Evilevitch V, Allen-auerbach MS, Eilber FC, Phelps ME, Czernin J, et al. Treatment Monitoring by  $^{18}F$ -FDG PET / CT in Patients with Sarcomas: Interobserver Variability of Quantitative Parameters in Treatment-Induced Changes in Histopathologically Responding and Nonresponding Tumors. *J Nucl Med.* 2008; 49(7): 1038 -46.
7. Lodge MA, Chaudhry MA, Wahl RL. Noise considerations for PET quantification using maximum and peak standardized uptake value. *J Nucl Med.* 2012; 53(7):1041-7.
8. Soret M, Bacharach SL, Buvat I. Partial-volume effect in PET tumor imaging. *J Nucl Med.* 2007; 48(6):932-45.
9. Nahmias C, Wahl LM. Reproducibility of standardized uptake value measurements determined by  $^{18}F$ -FDG PET in malignant tumors. *J Nucl Med.* 2008; 49(11):1804-8 .

10. Krak NC, Boellaard R, Hoekstra OS, Twisk JWR, Hoekstra CJ, Lammertsma AA. Effects of ROI definition and reconstruction method on quantitative outcome and applicability in a response monitoring trial. *Eur J Nucl Med Mol Imaging*. 2005; 32(3): 294-301.
11. Beyer T, Czernin J, Freudenberg LS. Variations in clinical PET/CT operations: results of an international survey of active PET/CT users. *J Nucl Med*. 2011; 52(2): 303-10.
12. Young H, Baum R, Cremerius U, Herholz K, Hoekstra O, Lammertsma AA, et al. Measurement of clinical and subclinical tumour response using [<sup>18</sup>F]-fluorodeoxyglucose and positron emission tomography: review and 1999 EORTC recommendations. European Organization for Research and Treatment of Cancer (EORTC) PET Study Group. *Eur J Cancer*. 1999; 35(13):1773-82.
13. Nakamoto Y, Zasadny KR, Minn H, Wahl RL. Reproducibility of common semiquantitative parameters for evaluating lung cancer glucose metabolism with positron emission tomography using 2-deoxy-2-[<sup>18</sup>F]fluoro-D-glucose. *Mol Imaging Biol*. 2002; 4(2):171-8.
14. Velasquez LM, Boellaard R, Kollia G, Hayes W, Hoekstra OS, Lammertsma AA, et al. Repeatability of <sup>18</sup>F-FDG PET in a multicenter phase I study of patients with advanced gastrointestinal malignancies. *J Nucl Med*. 2009; 50(10):1646-54.
15. Hashimoto N, Morita K, Tsutsui Y, Himuro K, Baba S, Sasaki M. Time-of-flight information improved the detectability of subcentimeter spheres using a clinical PET/CT scanner. *J Nucl Med Technol*. 2018; 46(3):268-73.
16. Rahmim A, Qi J, Sossi V. Resolution modeling in PET imaging: Theory, practice, benefits, and pitfalls. *Med Phys*. 2013; 40(6):064301.
17. Kidera D, Kihara K, Akamatsu G, Mikasa S, Taniguchi T, Tsutsui Y, et al. The edge artifact in the point-spread function-based PET reconstruction at different sphere-to-background ratios of radioactivity. *Ann Nucl Med*. 2016; 30(2):97-103.
18. Jaskowiak CJ, Bianco JA, Perlman SB, Fine JP. Influence of reconstruction iterations on <sup>18</sup>F-FDG PET/CT standardized uptake values. *J Nucl Med*. 2005; 46(3):424-8.
19. Maebatake A, Morita K, Akamatsu G, Tsutsui Y, Himuro K, Baba S, et al. The influence of minimal misalignment on the repeatability of PET images examined by the repositioning of point sources. *J Nucl Med Technol*. 2019; 47(1):55-9.
20. Fukukita H, Suzuki K, Matsumoto K, Terauchi T, Daisaki H, Ikari Y, et al. Japanese guideline for the oncology FDG-PET/CT data acquisition protocol: Synopsis of Version 2.0. *Ann Nucl Med*. 2014; 28(7): 693-705.
21. Munk OL, Tolbod LP, Hansen SB, Bogsrud T V. Point-spread function reconstructed PET images of sub-centimeter lesions are not quantitative. *EJNMMI Phys*. 2017; 4(1):1-12.
22. Rogasch JMM, Hofheinz F, Lougovski A, Furth C, Ruf J, Großer OS, et al. The influence of different signal-to-background ratios on spatial resolution and <sup>18</sup>F-FDG-PET quantification using point spread function and time-of-flight reconstruction. *EJNMMI Phys*. 2014; 1(1):1-16.
23. Thielemans K, Asma E, Ahn S, Manjeshwar RM, Deller T, Ross SG, et al. Impact of PSF modelling on the convergence rate and edge behaviour of em images in PET. *IEEE Nucl Sci Symp Conf Rec*. 2010; 3267-72.
24. Tong S, Alessio AM, Kinahan PE. Noise and signal properties in PSF-based fully 3D PET image reconstruction: An experimental evaluation. *Phys Med Biol*. 2010; 55(5): 1453-73.
25. Morey AM, Noo F, Kadrmas DJ. Effect of using 2mm voxels on observer performance for PET lesion detection. *IEEE Trans Nucl Sci*. 2016; 63(3):1359-66.
26. Akamatsu G, Mitsumoto K, Taniguchi T, Tsutsui Y, Baba S, Sasaki M. Influences of point-spread function and time-of-flight reconstructions on standardized uptake value of lymph node metastases in FDG-PET. *Eur J Radiol*. 2014; 83(1):226-30.
27. Adler S, Seidel J, Choyke P, Knopp M V, Binzel K, Zhang J, et al. Minimum lesion detectability as a measure of PET system performance. *EJNMMI Phys*. 2017; 4:13.
28. Boellaard R, Krak NC, Hoekstra OS, Lammertsma AA. Effects of noise, image resolution, and ROI definition on the accuracy of standard uptake values: A simulation study. *J Nucl Med*. 2004; 45(9): 1519-27.
29. Koopman D, van Dalen JA, Lagerweij MCM, Arkies H, de Boer J, Oostdijk AHJ, et al. Improving the detection of small lesions using a state-of-the-art time-of-flight PET/CT system and small-voxel reconstructions. *J Nucl Med Technol*. 2015; 43(1):21-7.
30. Wahl RL, Jacene H, Kasamon Y, Lodge MA. From RECIST to PERCIST: Evolving considerations for PET response criteria in solid tumors. *J Nucl Med*. 2009; 50(SUPPL. 1):122-50.

31. Kinahan PE, Perlman ES, Sunderland JJ, Subramaniam R, Wollenweber SD, Turkington TG, et al. The QIBA profile for

FDG PET/CT as an imaging biomarker measuring response to cancer therapy. *Radiology*. 2020; 294(2):647-57.